Evaluation of surface tension and Tolman length as a function of droplet radius from experimental nucleation rate and supersaturation ratio: Metal vapor homogeneous nucleation

A. A. Onischuk,[a] P. A. Purtov, A. M. Baklanov, and V. V. Karasev
Institute of Chemical Kinetics and Combustion, Novosibirsk 630090, Russia

S. V. Vosel
Institute of Mineralogy and Petrography, Novosibirsk 630090, Russia
and Institute of Chemical Kinetics and Combustion, Novosibirsk 630090, Russia

(Received 1 April 2005; accepted 1 November 2005; published online 5 January 2006)

Zinc and silver vapor homogeneous nucleations are studied experimentally at the temperature from 600 to 725 and 870 K, respectively, in a laminar flow diffusion chamber with Ar as a carrier gas at atmospheric pressure. The size, shape, and concentration of aerosol particles outcoming the diffusion chamber are analyzed by a transmission electron microscope and an automatic diffusion battery. The wall deposit is studied by a scanning electron microscope (SEM). Using SEM data the nucleation rate for both Zn and Ag is estimated as 10^{10} cm^{-3} s^{-1}. The dependence of critical supersaturation on temperature for Zn and Ag measured in this paper as well as Li, Na, Cs, Ag, Mg, and Hg measured elsewhere is analyzed. To this aim the classical nucleation theory is extended by the dependence of surface tension on the nucleus radius. The preexponent in the formula for the vapor nucleation rate is derived using the formula for the work of formation of noncritical embryo [obtained by Nishioka and Kusaka [J. Chem. Phys. **96**, 5370 (1992)] and later by Debenedetti and Reiss [J. Chem. Phys. **108**, 5498 (1998)]] and Reiss replacement factor. Using this preexponent and the Gibbs formula for the work of formation of critical nucleus the dependence of surface tension on the radius R_S of the surface of tension is evaluated from the nucleation data for above-mentioned metals. For the alkali metals and Ag the surface tension was determined to be a strong function of R_S. For the bivalent metals (Zn, Hg, and Mg) the surface tension was independent of radius in the experimental range. A new formula for the Tolman length δ as a function of surface tension and radius R_S is derived by integration of Gibbs-Tolman-Koenig equation assuming that δ is a monotonic function of radius. The formula derived is more correct than the Tolman formula and convenient for the elaboration of experimental data. Using this formula the values of δ are determined as a function of R_S from the experimental nucleation data. It is determined that all the metals considered are characterized by strong dependence of δ on radius; for the bivalent metals δ changes sign. © *2006 American Institute of Physics*. [DOI: 10.1063/1.2140268]

I. INTRODUCTION

The thermodynamic properties of interphase surface are fully characterized by a state function which is called surface tension σ. Therefore, when studying the colloid systems (formation process, thermodynamic stability, aging, etc.) the knowledge of surface tension as a function of droplet radius R is strictly necessary. In this paper we determined $\sigma(R)$ from the experimental data on Zn and Ag vapor homogeneous nucleations.

Our modern understanding of interfacial thermodynamics has its origins in the Gibbs theory of surface tension.[1] This theory considers a fluid maternal phase with i components and another fluid phase (with the same i components within it) being in equilibrium with the maternal one. This system is substituted to a hypothetical system composed of two homogeneous bulk phases (maternal phase α and another phase β) and a dividing surface, at the certain position. The key parameter in the Gibbs theory is surface tension σ attributed to a so-called surface of tension. The critical nucleus (i.e., the embryo which is in equilibrium with the maternal phase) is often extremely small in size so that the homogeneous bulk properties are not attained even at its center, but interfacial thermodynamics remains valid. The chemical potential of the bulk phase β is the same as that of the critical nucleus and the difference in pressure and composition between the nucleus and the phase β is incorporated in the value of the surface tension. Thus, to describe the thermodynamics of the interfacial system one should only know the surface tension and the location of the surface of tension.

In the case of spherical symmetry one can denominate the radius of the surface of tension R_S. As follows from the Gibbs theory the surface tension is a function of curvature. This dependence on curvature is governed by the Gibbs-Tolman-Koenig (GTK) differential equation:[2,3]

[a]Electronic mail: onischuk@ns.kinetics.nsc.ru

$$\frac{d[\ln \sigma(R_S)]}{d[\ln R_S]} = \frac{[2\delta(R_S)/R_S]\left[1+[\delta(R_S)/R_S]+\frac{1}{3}(\delta(R_S)/R_S)^2\right]}{1+[2\delta(R_S)/R_S]\left[1+[\delta(R_S)/R_S]+\frac{1}{3}(\delta(R_S)/R_S)^2\right]}, \quad (1)$$

where $\delta(R_S)$ is the so-called Tolman length which in the case of single-component system is equal to

$$\delta(R_s) = R_e - R_S, \quad (2)$$

R_e is the radius of the equimolar surface. Equation (1) may be written via the superficial density Γ of matter at the boundary between the phases α and β (computed with respect to the surface of tension),[2]

$$\frac{d[\ln \sigma(R_S)]}{d[\ln R_S]} = \frac{2\Gamma m}{R_S \Delta\rho}\left(1+\frac{2}{R_S}\frac{\Gamma m}{\Delta\rho}\right)^{-1}, \quad (3)$$

where $\Delta\rho$ (g/cm^3) is the difference between the densities of phases β and α, and m is the mass of molecules. If the function $\sigma(R_S)$ is known it is possible to solve Eq. (1) and determine the function $\delta(R_S)$. On the other hand, Eq. (2) gives the relationship between R_S and the real radius R_e; the last radius can be measured directly in the experiment.

Tolman believed[2] "that δ will be reasonably constant over a wide range of droplet sizes since it measures the distance between two surfaces whose separation is presumably closely connected with intermolecular distances in the liquid." Therefore, Tolman has solved the Eq. (1) treating δ as a constant and neglecting the terms δ/R_S and $\delta^2/3R_S^2$ in comparison with unity. This simplification resulted in Tolman's formula:

$$\sigma(R_S) = \sigma_\infty\left(1+\frac{2\delta}{R_S}\right)^{-1}, \quad (4)$$

where σ_∞ is the surface tension for planar interface. However, the last two decade papers (see, for example, Refs. 3–9) showed by numerical calculations that even for the simplest systems such as the Lennard-Jones (LJ) and Yukawa fluids as well as regular solutions δ strongly depends on the drop size. Thus, Tolman equation (4) is not correct. Recently Bartell[6] has derived an approximate equation which described good enough the LJ systems,

$$\delta(R_S) \approx \frac{k}{R_S} - \delta_\infty = \frac{k}{R_S} - \kappa\sigma_\infty, \quad (5)$$

where κ is the isothermal compressibility of the liquid, k is an undetermined integration constant depending upon physical properties of the system, and $\kappa\sigma_\infty$ is a fundamental length that is only weakly dependent on the nature of liquids[10,11] to be equal to $\kappa\sigma_\infty \approx 0.05a$, where $a \approx 3$–5 Å. The important features of Eq. (5) are δ is negative in sign and close to zero at large radiuses, and at small radiuses δ is a strong function of R_S.

Thus, the surface tension and the dependence of surface tension on curvature for the real systems are of primary interest in the interfacial thermodynamics. One of the possibilities to get an information on the surface tension is to extract it from the homogeneous nucleation rate. The expression for the nucleation rate defined as a number of critical nuclei formed per unit volume per unit time is

$$I = K_0 \exp\left(-\frac{W_{\text{crit}}}{k_B T}\right), \quad (6)$$

where k_B is the Boltzmann constant, T is temperature, and W_{crit} is the minimum work required to form a critical nucleus. As follows from the Gibbs theory of capillarity,[1]

$$W_{\text{crit}} = \frac{4\pi R_S^2 \sigma(R_S)}{3}. \quad (7)$$

The formula used in the classical nucleation theory (CNT) is not expression (7) but uses σ_∞ instead of $\sigma(R_S)$ and R_e instead of R_S which is a rough approximation. However, CNT has had a considerable success in predicting (usually qualitatively) the experimental supersaturations required to initiate homogeneous nucleation for a wide range of molecular fluids (see, for example, Refs. 12 and 13). Nevertheless, the theory is frequently in error when predicting actual nucleation rates.[14–16] In many experiments it was found that predictions of CNT differed from experimental by several orders of magnitude.[17–21]

The preexponential factor in Eq. (6) can be presented for the single-component system as:[22]

$$K_0 = 2R_e^2 n_1^2 (Y/m)^{1/2}, \quad (8)$$

where

$$Y = -\left(\frac{d^2 W}{dg^2}\right)_{g=g_{\text{crit}}}, \quad (9)$$

and n_1 is concentration of single molecules in vapor (cm^{-3}), g and g_{crit} are numbers of molecules in the droplet and critical droplet, respectively, and W is the reversible work of the formation of a noncritical droplet. Thus, to evaluate K_0 one should know W. One should note again that CNT uses σ_∞ and R_e instead of $\sigma(R_S)$ and R_S, respectively, when estimating W and Y which results in the following preexponential factor:[22]

$$K_0^{\text{CNT}} = n_1^2 \sqrt{\frac{2m\sigma_\infty}{\pi}}\frac{1}{\rho}, \quad (10)$$

where ρ (g/cm^3) denotes the density of the incompressible bulk phase β.

Recently Nishioka and Kusaka[23] and Debenedetti and Reiss[24] have extended the Gibbs treatment to noncritical nucleus by introducing a constraint that prevents the free transfer of matter between the embryo and the mother phase. Due to this constraint the embryo of arbitrary size can be considered as to be in equilibrium with the vapor phase. This formalism results in a new expression for the reversible work W of noncritical embryo formation the extrema conditions for which give Gibbs formula (7). The new expression for W gives the possibility to determine the value Y in (8) and, consequently, the rigorous expression for the nucleation rate. On the other hand, the rigorous expression for this rate gives

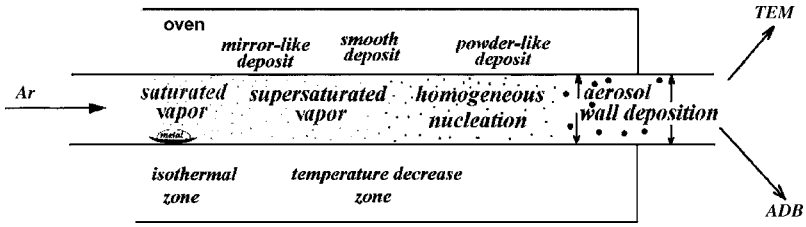

FIG. 1. Scheme of the laminar flow diffusion chamber.

the direct possibility to retrieve the surface tension $\sigma(R_S)$ and the radius of the surface of tension from the experimentally measured nucleation rate.

It is accepted now that a correction factor in the preexponent taking into account the Brownian motion of the cluster is necessary. The Lothe and Pound theory gave the correction factor 10^{14}–10^{17} (see Refs. 25–27). Reiss *et al.*[28] have argued that a careful calculation has led to an additional factor, but this coefficient is many orders of magnitude smaller than the Lothe and Pound factor. In the later paper[29] Reiss *et al.* have derived the expression for this correction factor K_R,

$$K_R \approx \frac{1}{Sn_1^{\mathrm{sat}}\sqrt{k_B T \kappa \mathsf{v}_g}}, \tag{11}$$

where n_1^{sat} is the saturated vapor concentration (cm^{-3}), S is the supersaturation ratio, and $\mathsf{v}_g = 4\pi R_e^3/3$ is the volume of the drop. The value of this factor varies in the range of 10^3–10^7 for typical systems studied in the literature such as H_2O, alcohols, saturated hydrocarbons, alkali metals (Li, Na, and Cs), and bivalent metals (Zn, Hg, and Mg). For Ag (Ref. 19) the correction factor is $K_R \approx 10^{11}$.

Metals are qualitatively different than molecular liquids due to the delocalized electrons in the bulk phase. The mobile electrons result in the oscillating dependence of cluster energy on the cluster size which gives relatively high concentration of magic size clusters with respect to antimagic ones.[30] This magic size effect gives an additional correction factor of about three orders of magnitude to the rate of nucleation. However, as it will be discussed in Sec. IV C this additional correction factor leads to a small error in the evaluation of the droplet surface tension. Therefore, taking into account the fact that there is still some uncertainty in the replacement correction factor K_R this magic size effect is out of the scope of this paper.

Thus, using Eqs. (6), (8), (9), and (11) and the expression for W by Nishioka and Kusaka[23] and Debenedetti and Reiss[24] one can evaluate the work of formation of critical nucleus from the experimentally measured nucleation rate at known temperature and supersaturation ratio. Then, using Gibbs formula (7) and the Kelvin equation:[23]

$$\ln S = \frac{2\sigma(R_S)m}{k_B T \rho R_S}, \tag{12}$$

one can determine the radius R_S of the surface of tension and the surface tension $\sigma(R_S)$ of critical nucleus.

This work is aimed at the evaluation of surface tension as a function of droplet radius for metals. In principle, the total cluster energy and surface tension can be determined by *ab initio* calculations for sufficiently large basis sets, but these calculations are nonrealistic for large enough clusters especially for heavy metals with many electrons and relativistic cores. However, just recently a paper[30] was published where the authors have used the jellium model which treats the atomic nuclei in the cluster and core electrons as uniform charge distribution providing a symmetric potential well for the valence electrons. These valence electrons were treated as an ideal Fermi gas moving in a spherical potential. It was found that the jellium model is able to evaluate the cluster energy for monovalent metals (Groups 1 and 11 of the Periodic Table). Treating this energy as free energy the nucleation onset pressure was calculated and a reasonable agreement with the experimental data for the alkali metals Li, Na, Cs, and Ag was found. Thus, the droplet energy and as a consequence surface tension can be estimated for alkali metals but this jellium model is not applicable for the higher valence metals.[30] Therefore, the only possibility to determine surface tension and the location of the surface of tension for multivalent metals droplets is to retrieve it from the experiment. In this paper we determined experimentally the nucleation rate and supersaturation at a known temperature for Zn to extract the droplet surface tension as a function of radius R_S. Besides, we elaborated other papers nucleation results for Li,[18] Na,[31,32] Cs,[33–35] Ag,[19] Hg,[36] and Mg (Ref. 37) to determine differences and common tendencies for the droplet surface tension and Tolman length.

II. EXPERIMENT

The main experimental results were obtained for Zn vapor nucleation. For comparison some measurements for Ag vapor nucleation were also done. Further in this section we will mainly describe the experimental procedure for Zn system. The data for Ag nucleation were obtained in the same manner as for Zn. The experiments on Zn and Ag vapor nucleations were carried out in a horizontal laminar flow diffusion chamber (Fig. 1). The nucleation chamber consisted of a horizontal quartz tube with the inner diameter of $d_{\mathrm{ch}} = 1.2$ and 1.4 cm in cases of Zn and Ag, respectively, and an outer oven. A flux of Ar was supplied to the inlet of the tube. Before entering the diffusion chamber the gas passed through a high efficiency Petrianov aerosol filter.[38] The Ar flow rate was 17 cm^3/s (at room temperature and atmospheric pressure). There was a saturation isothermal zone in the chamber where a crucible with metal was put (to create saturated vapor pressure) and a supersaturated vapor zone (temperature decrease zone), where the temperature was dropping down along the flow. In the last zone the vapor supersaturation S increased with the axial coordinate Z. Finally, at some coordinate the supersaturation reached the critical value resulting in homogeneous nucleation. The satu-

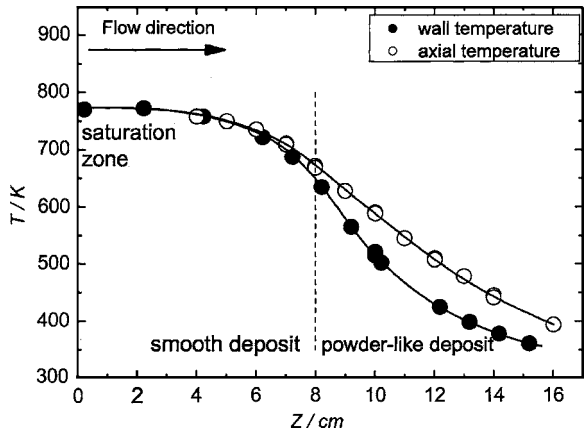

FIG. 2. Temperature profile in the laminar flow diffusion chamber.

ration zone temperature in Zn vapor experiments was varied in the range T_{sat}=750–900 K. A typical temperature profile is presented in Fig. 2. The axial and wall temperatures were measured by a *K*-type thermocouple. We assume that the vapor pressure was equal to the saturated vapor pressure in the saturation zone. This assumption was supported by the fact that there was a mirrorlike deposit at the beginning of temperature decrease zone testifying that a small decrease of temperature beyond the saturation temperature resulted in vapor supersaturation and as a consequence in wall vapor deposition. Another support to our assumption of vapor saturation is the independence of the experimental results on the metal surface area in the crucible.

The size and shape of Zn nanoparticles coming out of the diffusion chamber were studied by a transmission electron microscope (TEM). The sampling for TEM was carried out thermophoretically. The particles were deposited on an electron microscopy grid covered with polyvinyl formal film. The morphology of wall deposit was studied by a scanning electron microscope (SEM). To this end a thin quartz filament of diameter of 0.1 cm was fixed longitudinally on the inner surface of the diffusion chamber before the nucleation experiment. The experiment was held at a constant flow and temperature during time of 30–200 min. After the run the filament covered by the Zn deposit was removed from the flow chamber, cut to pieces, and the surface of these pieces was analyzed by SEM. Besides, the particle size spectrum and number concentration for the aerosol coming out of the diffusion chamber were measured by an automatic diffusion battery (ADB) coupled with a condensation nucleus counter.[39] This device is able to measure aerosol concentration in the range of 10^1–10^9 cm^{-3} and particle size distribution in the range of 2–200 nm.

III. RESULTS

Figure 3 shows aerosol number concentration and mean particle diameter as measured by the ADB at the outlet of the diffusion chamber for different saturation temperatures. Figure 4 demonstrates TEM images of particles sampled at the chamber outlet at different saturation temperatures. The particles seem to be crystalline. They have regular geometric shape; some particles have shapes of a stick. This regular

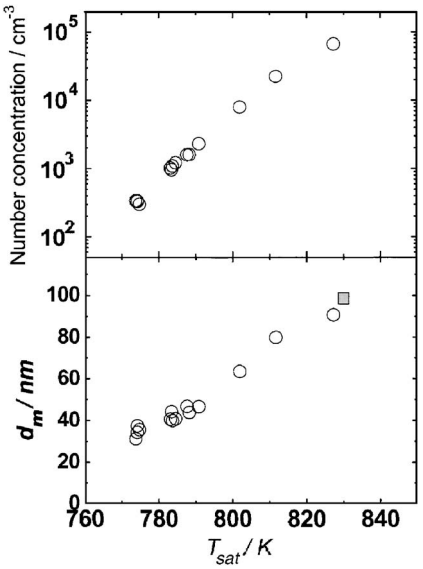

FIG. 3. Zn particle outlet concentration and mean diameter d_m (circles) vs vapor saturation temperature T_{sat} in the flow diffusion chamber (automatic diffusion battery measurements). The square symbol shows the mean diameter of particles deposited to the wall at the nucleation zone (SEM data).

shape is typical for aerosol particles of Zn and other metals.[40] Figure 5 demonstrates examples of Zn particle size spectra determined by the ADB measurement and TEM image elaboration.

The analysis of Zn deposit formed at the surface of quartz filament inserted to the diffusion chamber showed that there are two distinctly separated deposition zones characterized by a smooth and a powderlike deposit, respectively [Fig. 6(a)]. The nucleation rate is a strong function of supersaturation ratio; thus, we suppose that the position of border between the smooth and powderlike deposits corresponds to the zone of sharp increase of the nucleation rate. Figure 6(b) shows the deposit image for low deposition time and tem-

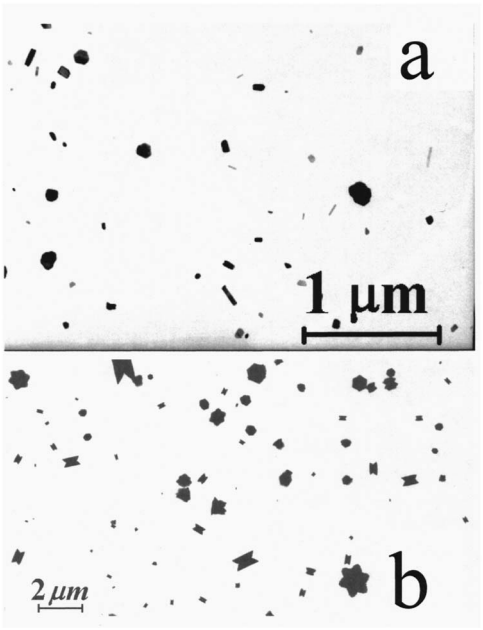

FIG. 4. TEM images of Zn particles sampled at the outlet of diffusion chamber. Vapor saturation temperature T_{sat}=780 (a) and 860 K(b).

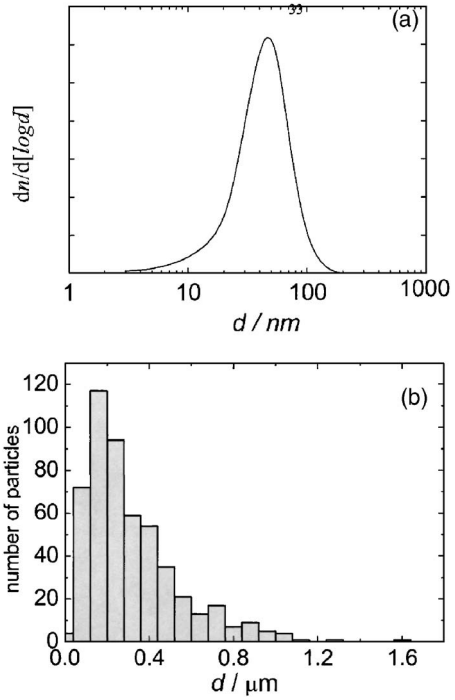

FIG. 5. Size distribution of Zn particles sampled at the outlet of the diffusion chamber (n is the number of particles and d is the particle diameter). (a) Automatic diffusion battery measurement, vapor saturation temperature $T_{sat}=795$ K; (b) TEM image elaboration result, $T_{sat}=860$ K.

perature. The border between the powderlike and smooth deposits is denoted by the coordinate Z_2. The smooth deposit (before Z_2) is formed by single particles and vapor deposition; the powderlike deposit consists of aggregates formed at the surface due to the overdeposition. Figure 6(c) shows the deposit profile measured by the light absorption. The linear dependence of the light absorption efficiency on the deposit density was checked in special experiments by cutting the quartz tube with deposit to pieces and weighing the deposit from each piece. One can see from the mass profile that the weight of the smooth deposit (before the coordinate Z_2) is about 1% of the total deposit mass. This means that the vapor depletion due to the wall deposition is negligible in the supersaturation zone. Therefore, to evaluate the supersaturation ratio one should not take into account the vapor wall deposition. The magnified SEM image of the powderlike deposit is given in Fig. 6(d). The image of deposit at the coordinate Z_2 is presented at Fig. 6(e). One can distinguish single particles which came to the wall from the nucleation zone. The frequency distribution for the diameters of these particles is shown in Fig. 6(f). The mean arithmetic diameter for particles deposited at Z_2 is 100 nm. It is of interest to compare the size of particles deposited to the wall near the nucleation zone with the size of particles outcoming the flow chamber. Figure 3 shows that at $T_{sat}=830$ K the outcoming particle diameter is the same as the deposited particle diameter (square symbol).

The nucleation rate (the number of nucleus formed in 1 s per 1 cm^3 at the axial coordinate Z_2 corresponding to the boundary between the smooth and powderlike deposits) was evaluated as 10^{10} cm^{-3} s^{-1}. In more detail the procedure of estimation of nucleation rate is given in Sec. IV A. We call the supersaturation ratio and temperature at the coordinate Z_2 as critical supersaturation and nucleation temperature, respectively. Changing experimentally the temperature of saturation we changed the location of Z_2 as well. As a result a new nucleation temperature and a critical supersaturation corresponded to the new location of Z_2. Thus, the critical supersaturation ratio S_{crit} as a function of nucleation temperature T_n was measured. Figure 7 demonstrates $\log_{10} S_{crit}$ vs Zn nucleation temperature. In case of Ag we measured $S=6000$ and $T_n=870$ K. This supersaturation ratio for Ag is compared with the data[19] in Fig. 8. One can see a reasonable agreement between the two sets of experimental data.

IV. DISCUSSION

A. Thermophoretic depletion of particles and nucleation rate

Taking into account that the saturated pressure of Zn vapor depends on temperature as[41]

$$\log_{10}[P_{sat}(\text{Torr})] = 8.35 - 6400/T, \tag{13}$$

one can estimate from Fig. 3 that only a small fraction of the initial saturated Zn vapor comes out of the nucleation chamber as aerosol; the rest is deposited to the walls as aerosol particles due to the thermophoresis. For example, for the saturation temperature $T_{sat}=830$ K we can estimate the vapor to outlet particles conversion ratio as:

$$\frac{[\text{part}]}{[\text{vapor}]}\frac{T_{\text{room}}}{T_{sat}} \approx 2\times 10^{-5}, \tag{14}$$

where [part] and [vapor] are the mass concentration of outlet particles and saturated vapor, respectively. The thermophoretic velocity u_T of particles in the free molecule regime can be estimated via the following expression:[42]

$$u_T = -0.55\nu\frac{\nabla T}{T}, \tag{15}$$

where ∇T is radial temperature gradient, and ν is the kinematic viscosity of the ambient gas (Ar) which can be approximated by the temperature dependence[41] $\nu=1.19\times 10^{-5}T^{1.65}$ cm^2/s. The average temperature gradient can be roughly estimated (see Fig. 2) as $\nabla T/T \approx 0.3$ cm^{-1}. Then, the thermophoretic velocity for the temperature of 500 K is about 0.06 cm/s. Assuming the parabolic flow velocity profile in the tube we estimated the characteristic thickness Δx of the layer near the wall from which the particles will come to the wall due to the thermophoresis during the residence time $t(\Delta x)\approx \Delta Z_{\text{therm}}/\nu_{\text{fl}}(\Delta x)$, where ΔZ_{therm} is the length of the zone of thermoforetic deposition (10 cm), and $\nu_{\text{fl}}(\Delta x)$ is the flow velocity (cm/s) at the distance Δx from the wall. Solving the equation $\Delta x = u_T t(\Delta x)$ we obtained $\Delta x \approx 0.05$ cm. Thus, the estimation shows that nucleation occurs near the walls in the layer of about 0.05 cm.

Figure 6(b) demonstrates the wall deposit formed at the vicinity of the nucleation zone at the temperature of 600 K. One can clearly see the locations of nucleation onset (Z_1) and powderlike deposit beginning (Z_2). The SEM images showed that the characteristic distance of nucleation development is $\Delta Z \approx 0.03$ cm. Assuming that the nucleation started at a dis-

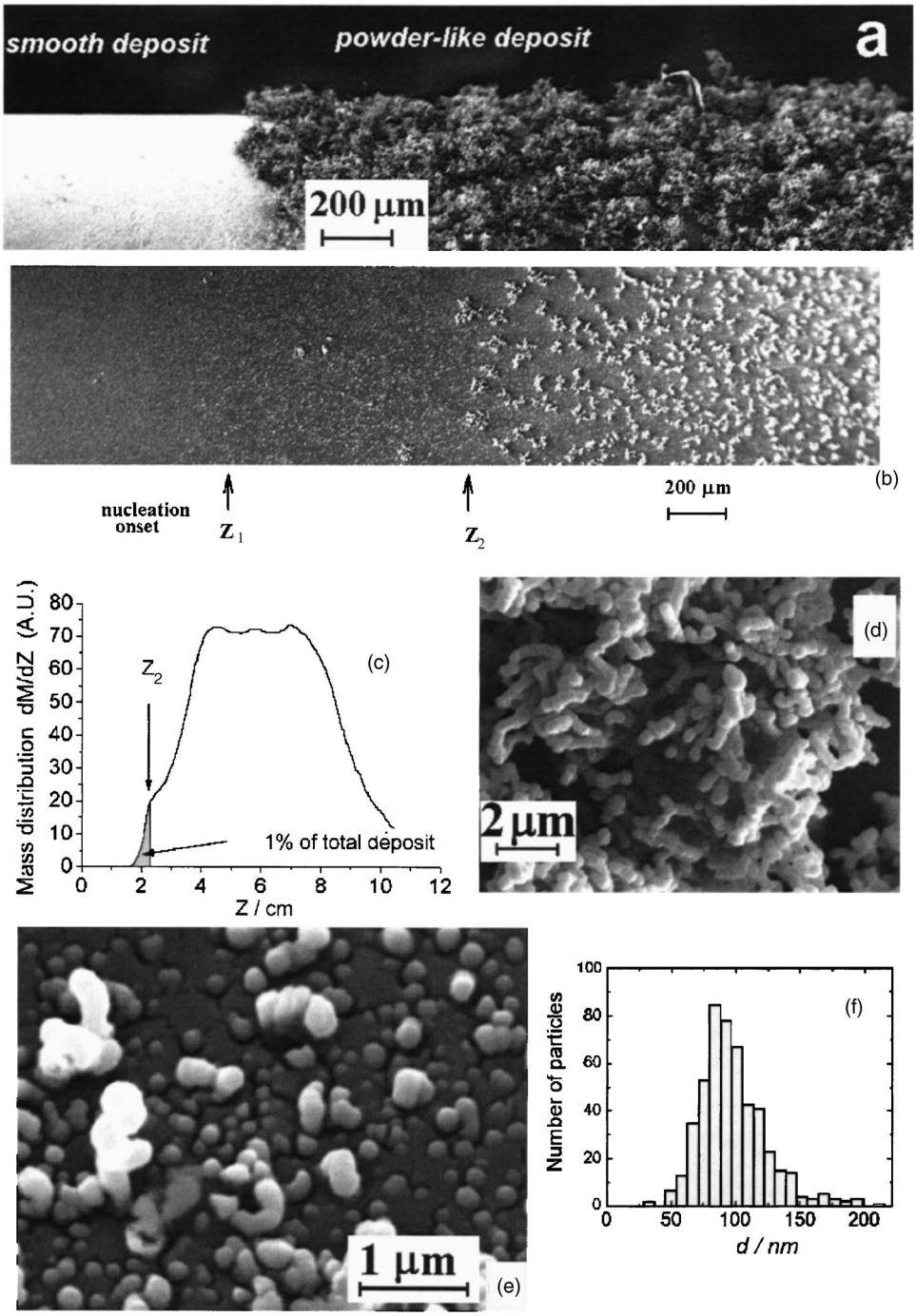

FIG. 6. SEM images of Zn wall deposit: Nucleation temperature is T_n=660 [(a) and (d)] and 600 K (b); (c) deposit mass (M) profile for conditions of (b); (e) SEM image from the border between the smooth and powderlike deposit regions T_{sat}=830 and T_n=690 K; (f) frequency distribution of the diameters of single particles presented in picture (e).

tance of 0.05 cm from the wall one can estimate Poisel's flow velocity at this distance (and T=600 K) to be ν_{fl}=10 cm/s. Thus, the characteristic nucleation time $t_{nucl} \approx \Delta Z/\nu_{fl} = 3\times10^{-3}$ s. As shown in Fig. 6(c) the mass of deposit in the range $Z<Z_2$ is about 1% of the total deposit. Thus, one can conclude that at the location Z_2 not more than 1% of initial vapor is converted to particles. The SEM and TEM analyses showed that the diameter of particles deposited to the wall at the nucleation region (at T_n=600 K) is of about 40 nm. Thus, taking into account the particle size, the vapor pressure at Z_2 (0.2 Torr) and vapor to particle conversion degree (1%) we estimate the concentration of particles at Z_2 to be $n \approx 2\times10^7$ cm^{-3} and the nucleation rate $I \approx n/t_{nucl} \approx 10^{10}$ cm^{-3} s^{-1}. Some supporting arguments for the estimated particle concentration can be found in Fig. 3 where the outlet concentration for particles with diameter of 40 nm is about 10^3 cm^{-3}. Taking into account the depletion coefficient 2×10^{-5} [see Eq. (14)] we get again the particle concentration in the nucleation zone to be about 5×10^7 cm^{-3}.

B. Homogeneous nucleation rate

Our task in this section is to obtain the expression for the homogeneous nucleation rate which takes into account the dependence of the droplet surface tension on radius, in other words, to obtain the formula for the preexponential factor in Eq. (6) using formulas (8) and (9) and the expression for

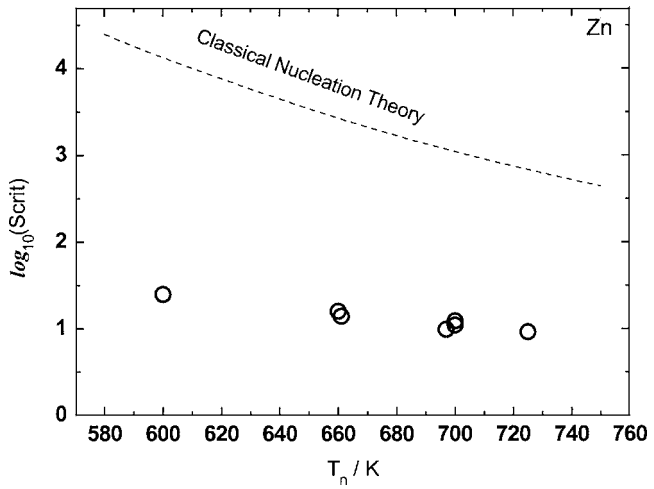

FIG. 7. Zn vapor supersaturation vs nucleation temperature. Circles: this work experimental data; dash line: classical nucleation theory prediction.

the work of formation of noncritical nucleus derived by Nishioka and Kusaka[23] and Debenedetti and Reiss.[24] Following Nishioka and Kusaka we consider a multicomponent system which is a liquid spherical drop surrounded by a vapor phase. In general the drop is not a critical nucleus. The total number of molecules for the component i in the system is specified as N_i to be governed by the following equation:

$$N_i = N_i^{\alpha} + N_i^{\beta} = \text{const}, \tag{16}$$

where N_i^{α} and N_i^{β} are the numbers of atoms in the real system belonging to the vapor and droplet, respectively. One of the main assumptions of the publication[23] is that the interfacial region is regarded as belonging to a drop. In other words, the chemical potential for surface molecules is equal to the chemical potential for the volume molecules of droplet.

Instead of the real system we consider now a hypothetical system composed of the two phases, liquid (noted as β), and vapor (noted as α) being uniform up to an imaginary

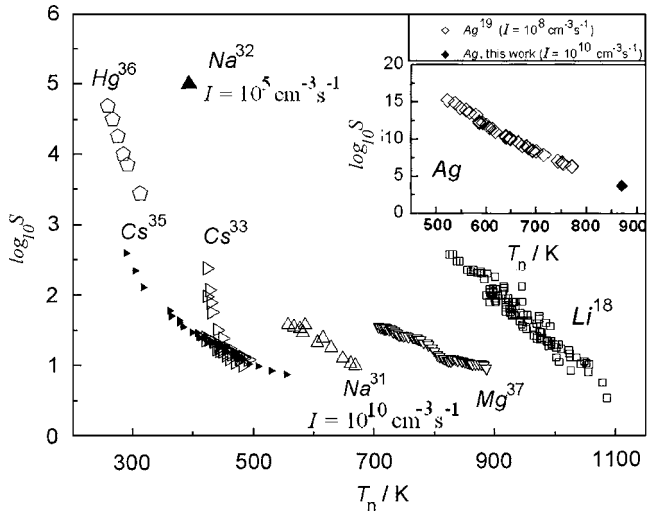

FIG. 8. Supersaturation vs nucleation temperature. Symbols: experimental data obtained in this work and elsewhere: Li,[18] Na,[31,32] Cs,[33,35] Ag,[19] Hg,[36] and Mg.[37]

geometrical surface that divides the two phases. We can specify the volumes of these phases as V_{α} and V_{β} which are governed by the following relationship:

$$V = V_{\alpha} + V_{\beta} = \text{const}. \tag{17}$$

In general the droplet and vapor chemical potentials of the two phases α and β are nonequal,

$$\mu_i^{\alpha} \neq \mu_i^{\beta}. \tag{18}$$

Following Gibbs the surface of tension was chosen as a dividing surface between two phases so that the fundamental equation has the following form:[23]

$$dE = TdS + \sum_i \mu_i^{\alpha} dN_i^{\alpha} + \sum_i \mu_i^{\beta} dN_i^{\beta} - P^{\alpha} dV^{\alpha} - P^{\beta} dV^{\beta} + \gamma dA, \tag{19}$$

where E is the energy, S is the entropy of the whole system, P^{α} and P^{β} are pressures of hypothetical homogeneous phases α and β, respectively, and γ and A are the surface tension and area of the surface of tension for the droplet which is a noncritical nucleus in the general case (for the critical nucleus we have denoted the surface tension by σ). For the spherical drop the variations of volume and surface are $dV_{\beta} = -dV_{\alpha} = 4\pi (R_S^{\text{nc}})^2 dR_S^{\text{nc}}$ and $dA = 8\pi R_S^{\text{nc}} dR_S^{\text{nc}}$, respectively, where R_S^{nc} is the radius of the surface of tension for a noncritical nucleus. As the system is assumed to be under a formal equilibrium the Laplace equation follows from Eq. (19),[23]

$$P^{\beta} - P^{\alpha} = \frac{2\gamma}{R_S^{\text{nc}}}. \tag{20}$$

It was shown in Ref. 23 as well as in Ref. 24 that the minimum work necessary to form a noncritical droplet in a multicomponent system and its variation at T, μ_i^{α}, and P^{α} being constant are

$$W = \sum_i N_i^{\beta} (\mu_i^{\beta} - \mu_i^{\alpha}) - V^{\beta} (P^{\beta} - P^{\alpha}) + \gamma A, \tag{21}$$

$$dW = \sum_i (\mu_i^{\beta} - \mu_i^{\alpha}) dN_i^{\beta} - (P^{\beta} - P^{\alpha}) dV^{\beta} + \gamma dA. \tag{22}$$

It follows from (20) and (22) that

$$dW = \sum_i (\mu_i^{\beta} - \mu_i^{\alpha}) dN_i^{\beta}. \tag{23}$$

The condition that a cluster formed is a critical nucleus is given by the extremity condition $dW = 0$ which results in the following equation:

$$\mu_i^{\beta} - \mu_i^{\alpha} = 0. \tag{24}$$

Under the condition (24) we have $\gamma = \sigma$ and $R_S^{\text{nc}} = R_S$. Therefore, substituting (24) to (21) and taking into account Laplace relation (20) we get well-known expression (7) for the minimum work of formation of the critical nucleus.

Equation (23) will be the starting point in our further discussion. This paper's experimental data are received for two-component Ar+Zn system. However, we assume that Ar gives negligible influence to the nucleation process. The only

effect from Ar gas is the increase of total pressure. Therefore we will apply to our nucleation process the single-component system formalism. For the single-component system Eq. (23) will transform to the following evident relation:

$$\frac{dW}{dN^\beta} = \mu^\beta(P^\beta) - \mu^\alpha(P^\alpha). \tag{25}$$

Using the condition of incompressibility and Laplace Eq. (20) and the previous notation for the number of molecules in droplet $N^\beta = g$ (see Introduction) we can rewrite Eq. (25),

$$\frac{dW}{dg} = \mu^\beta(P^\alpha) - \mu^\alpha(P^\alpha) + \frac{(P^\beta - P^\alpha)m}{\rho}$$

$$= \mu^\beta(P^\alpha) - \mu^\alpha(P^\alpha) + \frac{2\gamma m}{R_S^{\mathrm{nc}}\rho}. \tag{26}$$

The density ρ of the hypothetical phase β is linked with g and the radius of equimolar surface R_e^{nc} via the following equation:

$$\rho\tfrac{4}{3}\pi(R_e^{\mathrm{nc}})^3 = gm. \tag{27}$$

As mentioned in the Introduction our purpose in this section is to obtain the second derivative of W at the point $g = g_{\mathrm{crit}}$. Using (26) we get the second derivative of W (at constant ρ, T, and P^α) as

$$\frac{d^2W}{dg^2} = \frac{2m}{\rho}\frac{d}{dg}\left(\frac{\gamma}{R_S^{\mathrm{nc}}}\right). \tag{28}$$

Thus, to determine the second derivative of W one should know the derivative $d/dg(\gamma/R_S^{\mathrm{nc}})$ which can be presented as

$$\frac{d}{dg}\left(\frac{\gamma}{R_S^{\mathrm{nc}}}\right) = -\frac{\gamma}{(R_S^{\mathrm{nc}})^2}\frac{dR_S^{\mathrm{nc}}}{dg} + \frac{1}{R_S^{\mathrm{nc}}}\frac{d\gamma}{dg}. \tag{29}$$

To determine this derivative we will use the Gibbs-Duhem relation derived in Ref. 23,

$$-d\gamma = \Gamma^\alpha d\mu^\alpha + \Gamma^\beta d\mu^\beta, \tag{30}$$

where Γ^α and Γ^β are superficial densities governed by the following expressions:

$$4\pi R_S^2\Gamma^\alpha \equiv N^\alpha - N^{h\alpha} > 0, \tag{31}$$

$$4\pi R_S^2\Gamma^\beta \equiv N^\beta - N^{h\beta} < 0, \tag{32}$$

where $N^{h\alpha}$ and $N^{h\beta}$ are the numbers of molecules in the hypothetical homogeneous phases α and β, respectively. Let us consider the nonequilibrium process of deviation from the initial equilibrium state for the conditions of the α phase being kept invariant ($d\mu^\alpha = 0$). Then, we have from Eq. (30),

$$-d\gamma = \Gamma^\beta\frac{d\mu^\beta}{dP^\beta}\left(\frac{dP^\beta}{dg}\right)_{\mathrm{ne}}dg = \Gamma^\beta\nu_\beta\left(\frac{dP^\beta}{dg}\right)_{\mathrm{ne}}dg, \tag{33}$$

where ν_β is molar volume. On the other hand, for the equilibrium process of change of droplet radius ($d\mu^\alpha = d\mu^\beta$) we get from (30)

$$-d\sigma = (\Gamma^\alpha + \Gamma^\beta)\frac{d\mu^\beta}{dP^\beta}\frac{dP^\beta}{dg}dg = \Gamma\nu_\beta\frac{dP^\beta}{dg}dg, \tag{34}$$

where $\Gamma = \Gamma^\alpha + \Gamma^\beta$. Note, that Γ^α and Γ^β and other quantities in Eqs. (31) and (32) are attributed to the initial equilibrium state. The derivatives $(dP^\beta/dg)_{\mathrm{ne}}$ and dP^β/dg in Eqs. (33) and (34) correspond to the nonequilibrium and equilibrium processes of drop size change, respectively. From Eqs. (34) and (33) we obtain

$$\frac{d\gamma}{dg} = \frac{\Gamma^\beta}{\Gamma}\left(\frac{dP^\beta}{dg}\right)_{\mathrm{ne}}\left(\frac{dP^\beta}{dg}\right)^{-1}\frac{d\sigma}{dg}. \tag{35}$$

Thus, from Eqs. (29) and (35) we get

$$\frac{d(\gamma/R_S^{\mathrm{nc}})}{dg}$$

$$= -\frac{\gamma}{(R_S^{\mathrm{nc}})^2}\frac{dR_S^{\mathrm{nc}}}{dg} + \frac{1}{R_S^{\mathrm{nc}}}\frac{\Gamma^\beta}{\Gamma}\left(\frac{dP^\beta}{dg}\right)_{\mathrm{ne}}\left(\frac{dP^\beta}{dg}\right)^{-1}\frac{d\sigma}{dR_S}\frac{dR_S}{dg}$$

$$= -\frac{dR_S^{\mathrm{nc}}}{dg}\left(\frac{\gamma}{(R_S^{\mathrm{nc}})^2} - \frac{1}{R_S^{\mathrm{nc}}}\frac{\Gamma^\beta}{\Gamma}\left(\frac{dP^\beta}{dR_S^{\mathrm{nc}}}\right)_{\mathrm{ne}}\left(\frac{dP^\beta}{dR_S}\right)^{-1}\frac{d\sigma}{dR_S}\right). \tag{36}$$

At $g = g_{\mathrm{crit}}$ we get

$$\left(\frac{d(\gamma/R_S^{\mathrm{nc}})}{dg}\right)_{g=g_{\mathrm{crit}}} = -\frac{\sigma}{R_S^2}\left(\frac{dR_S^{\mathrm{nc}}}{dg}\right)_{g=g_{\mathrm{crit}}}\left(1 - \chi\frac{\Gamma^\beta}{\Gamma}\frac{d\ln\sigma}{d\ln R_S}\right), \tag{37}$$

where $\chi = (dP^\beta/dR_S^{\mathrm{nc}})_{R_S^{\mathrm{nc}}=R_S}(dP^\beta/dR_S)^{-1}$. The derivative $d(\ln\sigma)/d(\ln R_S)$ in Eq. (37) corresponds to equilibrium process (34) and is governed by Eq. (3). Thus, we rewrite Eq. (37) as

$$\left(\frac{d(\gamma/R_S^{\mathrm{nc}})}{dg}\right)_{g=g_{\mathrm{crit}}} = -\frac{\sigma}{R_S^2}\left(\frac{dR_S^{\mathrm{nc}}}{dg}\right)_{g=g_{\mathrm{crit}}}(1 + \chi\varphi), \tag{38}$$

where $\varphi = [2|\Gamma^\beta|m/(R_S\Delta\rho)]/[1 + 2\Gamma m/(R_S\Delta\rho)]$.

For the case when the phase β is liquid and the phase α is gas $\Delta\rho \approx \rho$. Then, the numerator of the fraction φ is [see Eq. (32)]

$$\frac{2|\Gamma^\beta|m}{R_S\Delta\rho} \approx 2\frac{4\pi R_S^2|\Gamma^\beta|m}{4\pi R_S^3\rho} = \frac{2}{3}\frac{N^{h\beta} - N^\beta}{N^{h\beta}} \ll \frac{2}{3}. \tag{39}$$

Taking into account that the denominator of the fraction φ is higher than unity when $|\Gamma^\alpha| > |\Gamma^\beta|$ (i.e., $(2/R_S)(\Gamma m/\Delta\rho) > 0$) and is about unity when $|\Gamma^\alpha| < |\Gamma^\beta|$ (because in this case $|(2/R_S)(\Gamma m/\Delta\rho)| < (2/R_S)(|\Gamma^\beta|m/\Delta\rho) \ll 2/3$) we get

$$\varphi \ll \tfrac{2}{3}. \tag{40}$$

Strict inequalities (39) and (40) can be violated when there are a few molecules in the drop, in other words, there should be at least one coordination sphere around the central molecule to satisfy (39) and (40). Taking into account that $P^\alpha \ll P^\beta$ we suppose that $\chi \approx 1$ which means that P^β is mainly determined by the surface tension and is weakly dependent of P^α. Thus, for the system vapor—incompressible liquid in the process of deviation from equilibrium state Eq. (38) is reduced to

$$\left(\frac{d(\gamma/R_S^{\rm nc})}{dg}\right)_{g=g_{\rm crit}} \approx -\frac{\sigma}{R_S^2}\left(\frac{dR_S^{\rm nc}}{dg}\right)_{g=g_{\rm crit}}. \quad (41)$$

One can see comparing Eqs. (29) and (41) that in effect γ may be treated as a constant equal to the equilibrium surface tension in taking the derivative from $\gamma/dR_S^{\rm nc}$.

To estimate the derivative $dR_S^{\rm nc}/dg$ in (41) we set

$$\frac{dR_S^{\rm nc}}{dg} \approx \frac{dR_e^{\rm nc}}{dg} = \frac{R_e^{\rm nc}}{3g}. \quad (42)$$

The last equation in (42) follows from Eq. (27).

Finally we obtain from (28), (41), and (42)

$$\left(\frac{d^2W}{dg^2}\right)_{g=g_{\rm crit}} \approx -\frac{8\pi R_e^4\sigma(R_S)}{9g_{\rm crit}^2R_S^2}. \quad (43)$$

Substituting (43) to (6)–(9) we have

$$I \approx n_1^2\sqrt{\frac{2m\sigma(R_S)}{\pi}}\frac{1}{\rho}\frac{R_e}{R_S}\exp\left(-\frac{4\pi R_S^2\sigma(R_S)}{3k_BT}\right). \quad (44)$$

Note, the preexponent in Eq. (44) is formally almost the same as CNT formula (10). The difference between these two factors is that the CNT expression includes the surface tension σ_∞ for the flat surface and Eq. (44) includes the surface tension $\sigma(R_S)$ related to the surface of tension for critical nucleus. Thus, Eq. (44) is an extension of the CNT expression for the vapor homogeneous nucleation rate which considers the curvature-dependent surface tension.

Finally, multiplying (44) to replacement correction factor K_R(11) and using Kelvin expression (12) we get

$$I \approx \frac{n_1^{\rm sat}S}{2\pi R_S}\sqrt{\frac{3\ln S}{\rho\kappa}}\exp\left(-\frac{16\pi m^2}{3\rho^2(\ln S)^2}\left(\frac{\sigma(R_S)}{k_BT}\right)^3\right). \quad (45)$$

Solving (45) together with (12) for certain temperature T we can evaluate the critical nucleus radius R_S and surface tension $\sigma(R_S)$ from known supersaturation ratio and nucleation rate.

C. Surface tension and Tolman length as a function of nucleus radius determined from the experimental supersaturation ratio and nucleation rate

Figures 7 and 8 present data on metal nucleation determined both in this paper and elsewhere.[18,19,31–33,35–37] The critical supersaturation for Zn vapor is compared with the CNT predictions. One can see a discrepancy of about two orders of magnitude between this paper experimental data and CNT calculated supersaturation. The data for Ag measured in Ref. 19 are consistent with the data determined in this paper as well as the results for Na determined in Refs. 31 and 32 looks to be in qualitative agreement.

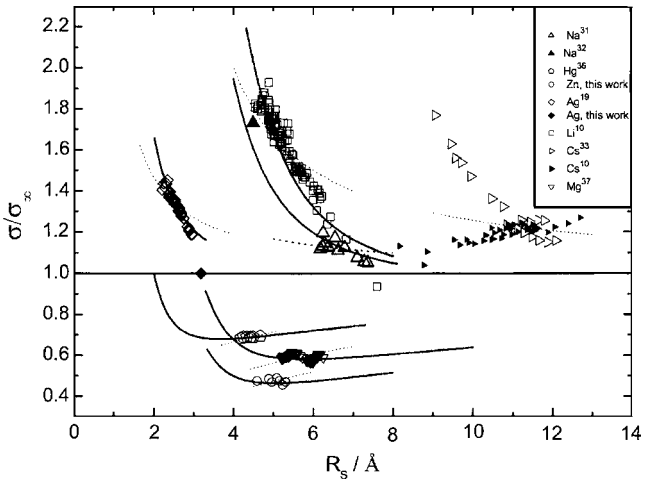

FIG. 9. Droplet surface tension σ to flat interface surface tension σ_∞ ratio vs radius R_S of the surface of tension as determined from the nucleation data (Figs. 7 and 8) by solving Eqs. (12) and (45) at fixed nucleation rates (see Table II). Solid lines are determined by the numerical integration of Gibbs-Tolman-Koenig Eq. (1) using Eq. (49) for the Tolman length and parameters χ and δ_∞ as given in Table III. Dotted lines correspond to Tolman equation (4) with $\delta=\delta_T$ (see the values of δ_T in Table II).

Solving (45) and (12) for fixed nucleation rate and temperature we can determine droplet surface tension as well as radius R_S of critical nucleus for each point in Figs. 7 and 8. In principle both σ and σ_∞ are functions of temperature but the ratio σ/σ_∞ can be considered as independent of temperature in the narrow temperature range. The evaluated ratios σ/σ_∞ are presented as functions of R_S in Fig. 9.

The important parameters used for evaluation of σ/σ_∞ are summarized in Table I. The temperature dependence of the planar interface surface tension is presented by

$$\sigma_\infty = \psi(T_0 - T), \quad (46)$$

where ψ and T_0 are parameters determined by fitting (46) to the dependencies of surface tension on temperature available from reference books (see, for example, Ref. 41). The temperature dependence of saturated vapor pressure is given by the following formula:

TABLE I. Important parameters for metals considered in this paper.

Metal	T_0/K	ψ/dyne cm^{-1} K^{-1}	C	D/K	ρ/(g/cm^3)	κ (cm^2/dyne)
Li	3300	0.140	8.00	8120	0.47	8.47×10^{-12}
Na	2350	0.100	7.70	5460	0.87	1.61×10^{-11}
Cs	1790	0.048	7.25	3920	1.75	5.0×10^{-11}
Ag	6980	0.161	8.92	14 464	9.35	9.03×10^{-13}
Hg	2540	0.210	8.04	3215	13.55	4.05×10^{-12}
Mg	3128	0.254	8.80	7674	1.59	5.06×10^{-12}
Zn	5430	0.167	8.35	6400	6.81	1.92×10^{-12}

TABLE II. Experimental nucleation data and evaluated R_S, $\delta(2R_S)$, N_S, β, and δ_T. R_S, $\delta(2R_S)$, and N_S (number of atoms confined by the surface of tension) were evaluated by the solution of Eqs. (12), (45), and (52) (at fixed nucleation rate as presented in the table). The ranges of S, R_S, $\delta(2R_S)$, and N_S correspond to the experimental ranges of T; δ_T=const was determined by the fitting of Tolman equation (4) to σ/σ_∞ (see Fig. 9).

	Experimental parameters			Evaluated parameters					
Metal	T/K	S	I ($cm^3\ s^{-1}$)	R_S/Å	$\delta(2R_S)$Å	N_S	β	δ_T/Å	References
Li	820–1100	400–10	10^9	4.5–6.8	−1.3 to−0.5	16–54	1.7	−1.00	18
Na	556–670	40–10	10^{10}	6.2–7.4	−0.5 to−0.2	23–39	1.2	−0.36	31
Na	393	10^5	10^5	4.5	−1.0	9		−0.95	32
Cs	290–550	400–8	0.1–1	8.2–12.7	~−1	18–68	1.0	−1.02	33 and 35
Ag	520–770	2×10^{15}–2×10^6	10^8	2.2–2.9	−0.4÷−0.2	2–5	1.0	−0.32	19
Ag	870	6000	10^{10}	3.2	0.0	7.2			This work
Hg	258–312	5×10^4–2×10^3	1	4.2–4.7	0.9–1.0	7–24	0.5	1.00	36
Mg	707–890	40–10	10^{10}	5.0–6.1	1.4–1.9	21–37	0.5	1.94	31 and 37
Zn	600–725	23–10	10^{10}	4.6–5.3	2.1–2.6	26–39	0.5	2.78	This work

$$\log_{10}(P_{\mathrm{sat}}(\mathrm{Torr})) = C - \frac{D}{T}, \tag{47}$$

where C and D are parameters determined by fitting (47) to the reference book data on saturated vapor pressure. The input data for evaluation of σ/σ_∞ are summarized in Table II.

One can see from Fig. 9 that all the metals considered can be divided into two groups Li, Na, Cs, and Ag (monovalent metals) and Mg, Zn, and Hg (bivalent metals). The alkali metals and Ag are characterized by the ratio $\sigma/\sigma_\infty > 1$. Li, Na, and Ag demonstrate a monotonic decrease of surface tension with R_S increasing. The plot σ/σ_∞ vs R_S for Na is very similar to that for Li. This similarity can be explained by the neighboring positions in the Periodic Table for these elements. The points for Cs are shifted to the right with regard to Li and Na which are probably related to the fact that the atomic radius for Cs (2.7 Å) is significantly larger than that for Li and Na (1.6 and 1.9 Å, respectively). The dependence of σ on R_S for Ag is similar to that for alkali metals (at least for Li and Na). Silver belongs to the Group 11 of the Periodic Table. The elements of this group have an electronic configuration $nS^1(n-1)d^{10}$ where n is the principal quantum number of the valence shell. The outermost S shell contains one electron and the d shells are fully filled and contracted. The nS electrons of these elements act similarly to the S electrons of the Group 1 metals.[30]

The data on Cs deserve a special consideration. The nucleation rate for Cs was measured in Ref. 33 as a function of supersaturation in the temperature range of 420–490 K using upward thermal diffusion cloud chambers. At temperatures less than 440 K the critical supersaturation increases dramatically with temperature decreasing (see Fig. 8). In Ref. 35 the nucleation rate was measured in the range of 290–550 K (solid triangles in Fig. 8) which demonstrated much weaker temperature dependency for the critical supersaturation at low temperature than it was found in Ref. 33. However, the dependence of surface tension on R_S is quite different for these two sets of experimental results measured in Refs. 33 and 35. The data[33] demonstrate the decrease of σ/σ_∞ with R_S increasing which is consistent with the data for other monovalent metals presented in Fig. 9. On the other hand, the results[35] demonstrate monotonic increase of σ/σ_∞ with R_S increasing which means that this function overpass a maximum somewhere at large R_S because it must come to unity finally. The authors[35] have measured more accurately the nucleation rate than it was done previously in Ref. 33, however, the disagreement of latest $\sigma(R_S)$ dependency for Cs with that for other monovalent metals is surprising. The explanation for this disagreement can be in overestimation of the nucleation rate in Ref. 35 for the low-temperature region, or in the fact that the properties of Cs are different from that for other monovalent metals considered in this paper.

The bivalent metals Zn, Hg, and Mg demonstrate $\sigma/\sigma_\infty < 1$. Moreover within the experimental accuracy the surface tension is independent on R_S for these elements in the studied range of critical nucleus radius. Probably the similar behavior of the function $\sigma(R_S)$ for Mg, Zn, and Hg is related to the similar electronic configuration ns^2.

We checked the sensitivity of the above method of evaluation of R_S and $\sigma(R_S)$ to the value of the preexponent in Eq. (45). To this aim the preexponent was increased by four orders of magnitude. The resulted magnitudes of both R_S and $\sigma(R_S)$ increased due to this variation by 6% for Li, Na, Ag, Zn, and Mg and by 4% for Hg and Cs which is within the experimental accuracy.

It is of interest to check if Tolman equation (4) is able to describe the dependence of σ/σ_∞ on R_S evaluated from the experimental nucleation rates. As seen from Fig. 9 the agreement between the Tolman equation predictions and our evaluation results is rather poor. Thus, the assumption of δ=const seems to be too rough. The values of Tolman length (δ_T=const) determined by fitting Eq. (4) to the quantities of σ/σ_∞ are summarized in Table II.

To find an approximate dependence of δ on R_S we simplify GTK differential Eq. (1) in the assumption of $\delta(R_S)/R_S$ being small with regard to unity and integrate it from $R_S=\infty$ corresponding to a plane surface to any radius R_S (in assumption that σ_∞ is known),

$$\ln\frac{\sigma(R_S)}{\sigma_\infty} \approx \int_\infty^{R_S} \frac{[2\delta(R_S)/R_S^2][1+\delta(R_S)/R_S]}{1+2\delta(R_S)/R_S} dR_S \approx \int_\infty^{R_S} [2\delta(R_S)/R_S^2][1-\delta(R_S)/R_S] dR_S. \tag{48}$$

One can see that the integral in Eq. (48) is mainly deter-

mined by the function $1/R_S^2$ so that the main contribution to this integral gives the region from R_S to about $3R_S$. In principle for approximate estimations δ in Eq. (48) can be substituted to some constant value approximately equal to $\delta(2R_S)$. But we perform more rigorous approach assuming that the dependence of δ on radius is governed by the following simple monotonic function:

$$\delta(R_S) = \frac{\chi}{R_S} + \delta_\infty, \tag{49}$$

where χ is constant, and δ_∞ is the Tolman length for the flat surface. One can see that function (49) is chosen as the two first terms of the Taylor-series expansion. In general case χ and δ_∞ can be both positive and negative. Though formula (49) is relatively simple it is able to describe all the possible types of monotonic tendencies. Function (49) gives strong dependence on radius for small particles and asymptotic approach to the value δ_∞. Formally relationship (49) is the same as Bartell's formula (5) determined for the LJ systems. Substituting (49) to (48) we get

$$\ln\frac{\sigma(R_S)}{\sigma_\infty} = -\frac{2}{R_S}\left(\frac{\chi}{2R_S}+\delta_\infty\right) + \frac{2}{R_S^2}\left[\left(\frac{\chi}{2R_S}+\delta_\infty\right)^2 - \frac{\delta_\infty}{2}\left(\frac{\chi}{1.5R_S}+\delta_\infty\right)\right]. \tag{50}$$

Taking into account (49) we rewrite Eq. (50) as

$$\ln\frac{\sigma(R_S)}{\sigma_\infty} = -2\frac{\delta(2R_S)}{R_S}\left(1-\frac{\delta(2R_S)}{R_S}\beta\right), \tag{51}$$

where $\beta=(1-(1/2)(\delta_\infty\delta(1.5R_S)/\delta^2(2R_S)))$. In the case when $|\delta_\infty| \ll |\delta(2R_S)|$, which, in particular, corresponds to the LJ fluids, we have $\beta\approx 1$. In the case $\delta_\infty > \delta(2R_S) > \delta(1.5R_S) > 0$ one gets $\beta\approx 0.5$. One can see from Eq. (51) that $\sigma(R_S)$ is mainly determined by $\delta(2R_S)$ as foreseen above. Multiplying Eq. (51) by $1+\beta\delta(2R_S)/R_S$ we have for $(\beta\delta(2R_S)/R_S)^2 \ll 1$,

$$\frac{\delta(2R_S)}{R_S} \approx -\frac{\ln\sigma(R_S)/\sigma_\infty}{2+\beta\ln\sigma(R_S)/\sigma_\infty}. \tag{52}$$

One should note that Eq. (52) is a more exact formula than the Tolman expression because this formula was derived by integrating Eq. (48) which contains one more linear term with regard to the Tolman's integration procedure,[2] besides, δ is a function of radius in our integration. The important feature of Eq. (52) is that it does not include directly the values of χ and δ_∞. Thus, using Eq. (52) one can determine $\delta(2R_S)$ directly from $\sigma(R_S)/\sigma_\infty$ presented in Fig. 9.

On the other hand, taking the derivative $[d/d(\ln R_S)] \times(\ln[\sigma(R_S)/\sigma_\infty])$ from Fig. 9 one can determine $\delta(R_S)$ using GTK Eq. (1). However, as one can see from Fig. 9, due to the experimental error the quantities σ/σ_∞ are determined with the standard deviation of about 10%. This experimental error results in the accuracy of evaluation of quantity $[d/d(\ln R_S)](\ln\sigma(R_S)/\sigma_\infty)$ to be 50% at the ends of the experimental range and 10% at the middle part of the range of R_S. Therefore, we used Eq. (1) to determine directly $\delta(R_S)$ only at the middle point of the range of R_S to be consistent with the accuracy of the quantities $\sigma(R_S)/\sigma_\infty$. It seems as if one

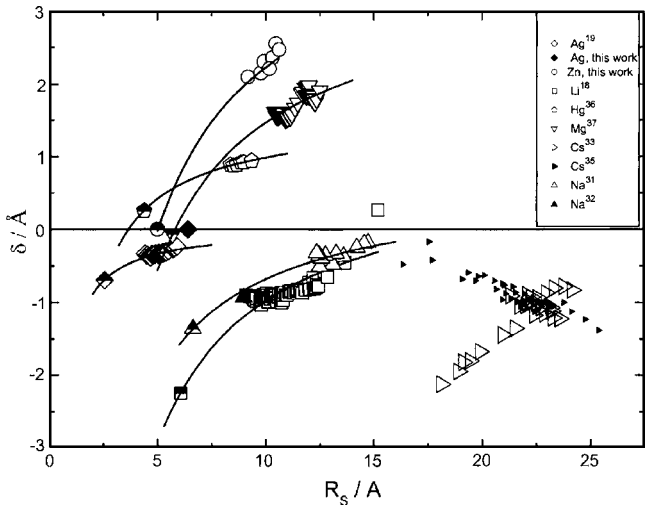

FIG. 10. Tolman length δ vs radius of the surface of tension as determined from σ/σ_∞ data (Fig. 9) using Eq. (52): open and solid symbols, and Gibbs-Tolman-Koenig Eq. (1): semifilled symbols. Solid lines are governed by Eq. (49) with χ and δ_∞ as given in Table III.

and the same Eq. (1) gives information on both the quantity $\delta(R_S)$ which is contained by (1) directly and the quantity $\delta(2R_S)$ which is not contained by Eq. (1). However, in fact $\delta(2R_S)$ is calculated from integral GTK Eq. (48) which contains more information than Eq. (1) because the integral equation includes the quantity σ_∞.

The values of δ are presented in Fig. 10. Semifilled symbols correspond to direct calculation by differential GTK Eq. (1) for each metal except for Cs (for which the above derivative is uncertain). Open symbols [and two filled symbols for Na (Ref. 32) and Ag (this work)] correspond to evaluation by Eq. (52). When evaluating $\delta(2R_S)$ for Li and Na we determined β in (52) by consecutive approximations using $\beta_0=1$ at the initial step. Then the plot including points for both $\delta(R_S)$ and $\delta(2R_S)$ was fitted by Eq. (49). After this a new value ofβ for the next approximation was determined. The values of β determined for Li and Na in this approximation process are given in Table II. In the case of Ag the initial approximation $\beta_0=1$ was enough. In the cases of Zn, Hg, and Mg we set $\beta=0.5$ and for Cs $\beta=1.0$. The determined quantities δ were fitted by Eq. (49) (solid lines in Fig. 10) with the values of χ and δ_∞ as given in Table III.

Alkali metals Li and Na demonstrate the dependence of δ on R_S which is akin to that for Ag (δ is negative in sign and the absolute value of δ decreases monotonically with R_S). However, Ag is much more similar to LJ systems than Li and Na because $\delta_\infty\approx 0$ for Ag as in contrast with Li and Na (see Table III). This similarity between Ag and LJ systems correlates with the fact that both the Group 11 elements (Cu, Ag, and Au) and the Group 18 elements have the same fcc type of crystal lattice as in contrast with the Group 1 elements which have bcc crystalline structure. The dependence of δ on R_S for the bivalent metals is quite different from that for the monovalent metals. Zn, Mg, and Hg show δ close to zero at $R_S\approx 5$ Å and positive δ increasing with R_S at higher radii.

To check the accuracy of evaluation of δ we integrated numerically GTK Eq. (1) substituting Eq. (49) for δ and using χ and δ_∞ presented in Table III. The integration results

TABLE III. The values of χ and δ_∞ from Eq. (49) which govern the solid lines in Figs. 9 and 10.

Metal	χ/Å^2	δ_∞/Å
Li	−19.45	0.97
Na	−13.51	0.67
Ag	−1.96	0.07
Hg	−5.71	1.56
Mg	−20.30	3.50
Zn	−22.50	4.48

are given as solid lines in Fig. 9. One can see that there is a good agreement between symbols and lines indicating the validity of formula (52) within the experimental accuracy and to the fact that our approximation [Eq. (49)] is sufficient. One can see also that the curve calculated for Na (Ref. 31) is in reasonable agreement with the point for Na.[32]

Thus, the knowledge of the function $\delta(R_S)$ allows one to reconstruct the function $\sigma(R_S)$ in the range wider than the experimental area. It is important to note also that the calculated σ/σ_∞ curves come through a minimum for the bivalent metals demonstrating a strong increase with R_S decreasing at small values of the radius and approaching to unity at large R_S. Thus, the surface tension values for bivalent metals as determined from the experiment are found to be in the minimum of the function $\sigma(R_S)$ which evidently corresponds to the lowest potential barrier in nucleation process. The minimum of the function $\sigma(R_S)$ is caused by the change of sign of δ for the Zn, Mg, and Hg. As seen from Eq. (1) this change of sign could be foreseen just from the fact of $d\sigma/dR_S \approx 0$ for these metals as demonstrated in Fig. 9. The question of possibility that δ might change sign is discussed in the literature.[2]

One can see from Fig. 9 that Tolman equation (4) is applicable for small droplets only in a very narrow range of nucleus size at some fixed δ which we denoted as δ_T. The range of size under consideration can be characterized by the mean radius R_S^{mean}. Comparing δ_T with $\delta(2R_S)$ (see Table II) one can find out that

$$\delta_T \approx \delta(2R_S^{\text{mean}}). \tag{53}$$

When $\delta(2R_S)/R_S \ll 1$ relationship (53) follows from Eq. (51); indeed, under this condition the second term in the brackets of the right-hand side of Eq. (51) vanishes. Then expanding $\ln(\sigma(R_S)/\sigma_\infty)$ in a Taylor series around $\sigma(R_S)/\sigma_\infty = 1$ we get

$$\sigma(R_S) = \sigma_\infty \left(1 + \frac{2\delta(2R_S)}{R_S}\right)^{-1}, \tag{54}$$

which is formally the same as Tolman formula (4) with the only difference that Eq. (54) includes the function $\delta(2R_S)$ while (4) contains δ=const. Thus to estimate σ for R_S by the Tolman formula one should use δ for $2R_S$. For a narrow range of droplet size one can use $\delta(2R_S^{\text{mean}})$ in Eq. (54) and obtain relationship (53). There is a discussion in the literature about the range of applicability of Tolman Eq. (4) (see, for example, Ref. 5). The accepted point of view is that the Tolman length in (4) is defined as δ_∞. The density-functional calculations[5] for LJ systems show that under the assumption $\delta = \delta_\infty$ the Tolman equation is not valid when the droplet holds less than 10^6 molecules. The last fact is not surprising because as shown above to evaluate $\sigma(R_S)$ for small droplets one should substitute δ=const in the Tolman equation to $\delta(2R_S)$ which is much larger than δ_∞ for LJ systems.

V. CONCLUSIONS

Zinc and silver vapor homogeneous nucleations are studied experimentally at the temperatures from 600 to 725 and 870 K, respectively, in a laminar flow diffusion chamber with Ar as a carrier gas at atmospheric pressure. Using SEM data the nucleation rate for both Zn and Ag is estimated as 10^{10} cm^{-3} s^{-1}. The vapor critical supersaturation is measured as 25–9 for Zn vapor and 6000 for Ag.

A new approach for the evaluation of the droplet surface tension as a function of radius from the experimental homogeneous nucleation rate and supersaturation ratio is developed. To determine the droplet surface tension we extended the classical nucleation theory (CNT). As a result the preexponent in the expression for the nucleation rate was derived (for the case of gaseous maternal phase) using the formula for the work of formation of noncritical embryo (obtained by Nishioka and Kusaka[23] and Debenedetti and Reiss[24]). At some simplification this preexponent looks formally almost the same as in the CNT formula with the difference that the new expression includes the surface tension for nucleus as in contrast to CNT formula which involves the surface tension for flat surface. Using the extended formula we retrieved the dependence of surface tension on the radius of surface of tension R_S from the nucleation rate and supersaturation ratio determined experimentally at certain temperatures for Zn and Ag (measured in this paper) as well as Li, Na, Cs, Ag, Mg, and Hg (measured elsewhere). It is found that the monovalent metals are characterized by the relationship $\sigma/\sigma_\infty > 1$ and monotonic decrease of surface tension with R_S increasing (at least Li, Na, and Ag); the surface tension for the bivalent metals is governed by the relationship $\sigma/\sigma_\infty = \text{const} < 1$.

To evaluate the Tolman length as a function of droplet radius we simplified and integrated the Gibbs-Tolman-Koenig equation assuming that δ is the monotonic function of radius (49). This approximation resulted in the relationship between the Tolman length and the surface tension [Eq. (52)]; one can obtain the function $\delta(2R_S)$ directly from the quantity $\sigma(R_S)$ determined experimentally. Using formulas (52) and (1) we retrieved the dependence of δ on R_S from the dependencies of σ on R_S determined for the above-mentioned elements. Equation (52) is more correct than Tolman formula (4), because we did not neglect the linear term in the numerator of GTK equation as in contrast with Tolman;[2] besides we considered δ to be a function of the droplet radius. We found that all the elements are characterized by a strong dependence of δ on radius. In the cases of Li, Na, Cs, and Ag (monovalent metals) δ is negative in sign and its absolute magnitude increases with radius (at least for Li, Na, and Ag). For Ag $\delta_\infty \approx 0$ like in the case of the Lennard-Jones systems. This similarity between Ag and LJ fluids can be explained by the fact that both Ag and LJ sys-

tems have the same fcc type of crystal lattice. The dependence of δ on R_S for the bivalent metals is quite different from that for the monovalent metals. Zn, Mg, and Hg show δ close to zero at $R_S \approx 5$ Å and a positive δ increasing with R_S at higher radii.

To check the accuracy of the Eq. (52) we calculated $\sigma(R_S)$ by integrating numerically GTK Eq. (1) using the evaluated functions $\delta(R_S)$. A good agreement was found between the calculated dependencies $\sigma(R_S)$ and the values of surface tension as determined from the experimental data. The calculated σ/σ_∞ curves come through a minimum for the bivalent metals demonstrating a strong increase with R_S decreasing at small values of the radius and approaching to unity at large R_S. Thus, the surface tension values for bivalent metals as determined from the experiment are found to be in the minimum of the function $\sigma(R_S)$ which evidently corresponds to the lowest potential barrier in the nucleation process. The minimum of the function $\sigma(R_S)$ is caused by the change of sign of δ for Zn, Mg, and Hg. As seen from Eq. (1) this change of sign could be foreseen just from the fact that $d\sigma/dR_S \approx 0$ for these metals as demonstrated in Fig. 9.

ACKNOWLEDGMENTS

Financial support for this work was provided by the Presidium of Russian Academy of Sciences (Project No. 8.23), INTAS foundation (Grant No. 03-53-5203), Russian Foundation for Basic Research (RFBR) (Project Nos. 04-03-33162, 04-03-33163, 05-03-90576-NSC_a, and 05-02-08290-OFI_a), NSC(Taiwan)-RFBR No. 94WFA0600016 (Contract No. RP05E15), and Program of Russian Academy of Sciences, subprogram 4.2.4. The authors are grateful to A. Sadykova for his help in the experiment.

[1] J. W. Gibbs, *Thermodynamics and Statistical Mechanics* (Nauka, Moscow, 1982).
[2] R. C. Tolman, J. Chem. Phys. **17**, 333 (1949).
[3] K. Nishioka, H. Tomino, I. Kusaka, and T. Takai, Phys. Rev. A **39**, 772 (1989).
[4] A. H. Falls, L. E. Scriven, and H. T. Davis, J. Chem. Phys. **75**, 3986 (1981).
[5] K. Koga, X. C. Zeng, and A. K. Shchekin, J. Chem. Phys. **109**, 4063 (1998).
[6] L. S. Bartell, J. Phys. Chem. B **105**, 11615 (2001).
[7] V. Talanquer and D. W. Oxtoby, J. Phys. Chem. **99**, 2865 (1995).
[8] R. Guermeur, F. Biquard, and C. Jacolin, J. Phys. Chem. **82**, 2042 (1985).
[9] H. Tomino, I. Kusaka, and K. Nishioka, J. Cryst. Growth **113**, 633 (1991).
[10] P. A. Egelstaff and B. Widomj, J. Chem. Phys. **53**, 2667 (1970).
[11] S. W. Mayer, J. Phys. Chem. **67**, 2160 (1963).
[12] J. L. Katz, P. Mirabel, C. J. Scoppa II, and T. L. Virkler, J. Chem. Phys. **65**, 382 (1976).
[13] M. P. Anisimov, V. G. Kostrovskij, and M. S. Shtein, Colloid J. USSR **40**, 317 (1978).
[14] B. Donn and J. Nuth, Astrophys. J. **288**, 187 (1985).
[15] J. D. Gunton, J. Stat. Phys. **95**, 903 (1999).
[16] C. Becker, J. Chem. Phys. **72**, 4579 (1980).
[17] C. C. M. Luijten, P. Peeters, and M. E. H. van Dongen, J. Chem. Phys. **111**, 8535 (1999).
[18] F. T. Ferguson and J. A. Nuth III, J. Chem. Phys. **113**, 4093 (2000).
[19] J. A. Nuth, K. A. Donnelly, B. Donn, and L. U. Lilleleht, J. Chem. Phys. **85**, 1116 (1986).
[20] A. Dillmann and G. E. A. Meier, J. Chem. Phys. **94**, 3872 (1991).
[21] C. F. Deale and G. E. A. Meier, J. Chem. Phys. **98**, 9850 (1993).
[22] Ya. I. Frenkel, *Kinetic Theory of Liquids* (Academy of Sciences, Moscow-Leningrad, 1959).
[23] K. Nishioka and I. Kusaka, J. Chem. Phys. **96**, 5370 (1992).
[24] P. G. Debenedetti and H. Reiss, J. Chem. Phys. **108**, 5498 (1998).
[25] J. Lothe and G. M. Pound, J. Chem. Phys. **45**, 630 (1966).
[26] J. Lothe and G. M. Pound, J. Chem. Phys. **36**, 2080 (1962).
[27] V. Ruth, J. P. Hirth, and G. M. Pound, J. Chem. Phys. **88**, 7079 (1988).
[28] H. Reiss, J. L. Katz, and E. R. Cohen, J. Chem. Phys. **48**, 5553 (1968).
[29] H. Reiss, W. K. Kegel, and J. L. Katz, J. Phys. Chem. A **102**, 8548 (1998).
[30] R. Badahur and R. B. McClurg, J. Chem. Phys. **121**, 12499 (2004).
[31] D. M. Martinez, F. T. Ferguson, R. H. Heist, and J. A. Nuth III, J. Chem. Phys. **115**, 310 (2001).
[32] J. Hecht, J. Appl. Phys. **50**, 7186 (1979).
[33] G. -S. Cha, H. Uchtmann, J. A. Fisk, and J. L. Katz, J. Chem. Phys. **101**, 459 (1994).
[34] J. A. Fisk, M. M. Rudek, J. L. Katz, D. Beiersdorf, and H. Uchtmann, Atmos. Res. **46**, 211 (1998).
[35] M. M. Rudek, J. L. Katz, and H. Uchtmann, J. Chem. Phys. **119**, 11505 (1999).
[36] H. Uchtmann, K. Rademann, and F. Hensel, Ann. Phys. **48**, S207 (1991).
[37] F. T. Ferguson, J. A. Nuth III, and L. U. Lilleleht, J. Chem. Phys. **104**, 3205 (1996).
[38] A. A. Kirsch, I. B. Stechkina, and N. A. Fuchs, J. Aerosol Sci. **5**, 119 (1975).
[39] A. Ankilov, A. Baklanov, R. Mavliev, and S. Eremenko, J. Aerosol Sci. **22**, S.325 (1991).
[40] E. R. Buckle, K. Jagath, A. Mawella, and P. Tsakiropoulos, J. Colloid Interface Sci. **112**, 42 (1986).
[41] *Physical Magnitudes*, edited by I. S. Grigoriev and E. Z. Meylikhov (Energoatomizdat, Moscow, 1991).
[42] *Aerosol Measurement: Principles, Techniques, and Applications*, edited by P. A. Baron and K. Willeke (Wiley-Interscience, New York, 2001).